PCCP

PAPER

View Article Online
View Journal | View Issue

Check for updates

Cite this: *Phys. Chem. Chem. Phys.*, 2025, **27**, 17852

Investigating halogen bonds in substituted graphitic carbon nitride through vibrational spectroscopy

Daniel P. Devore, † Thomas L. Ellington ‡ and Kevin L. Shuford *

Received 23rd June 2025,
Accepted 5th August 2025

DOI: 10.1039/d5cp02395e

rsc.li/pccp

The graphitic carbon nitride (g-C_3N_4) triazine backbone was substituted with OH, SH, and PH_2 substituents to examine its potential for halogen bonding applications. A series of four halogen bond (XB) donors were systematically complexed with substituted triazine units in a series of 1 : 1, 2 : 1, and 3 : 1 XB donor : acceptor complexes for comparison studies. These XB acceptor units offered stabilizing hydrogen bonding sites in addition to the halogen bonding sites, depending upon the position the XB donor bonded to the acceptor. The addition of one XB donor to each acceptor in the 1 : 1 and 2 : 1 XB complexes was shown to have ≥90% additivity to the binding energies. Local mode analysis was performed for further comparison of the halogen and hydrogen bonds formed, concluding that these interactions are XB dominated with supportive hydrogen bond interactions.

Open Access Article. Published on 05 August 2025. Downloaded on 5/7/2026 3:16:31 AM.
This article is licensed under a Creative Commons Attribution 3.0 Unported Licence.

Introduction

Non-covalent interactions (NCIs), such as intermolecular halogen bonding, have taken a firm hold in the fields of biology and drug design,[1–4] catalysis,[5] crystal engineering,[6–10] materials science,[7,9] and synthetic chemistry.[5,11,12] A halogen bond (XB), which is similar to a hydrogen bond (HB)[13,14] and a chalcogen bond (ChB),[12,15–22] is a weak interaction that occurs due to the electrophilic (electron accepting) nature of covalently-bonded halogen atoms in XB donors interacting with nucleophilic (electron donating) sites on nearby XB acceptors. The positive region that is formed on the halogen atom opposite of the covalent bond was originally defined to be due to the half-filled p_z orbital in the halogen atom[23] and was later explained to occur as a result of the depletion of electron density due to the anisotropic redistribution of electron density upon the formation of a covalent (R–X) bond between a halogen atom and some other atom is called the σ-hole.[24] This redistribution of electron density, also known as polar flattening,[24–26] forms a "belt" of negative ($\delta-$) electrostatic potential that can act as an electron donor for concurrent hydrogen or halogen bond interactions.[27–38] Fig. 1 displays the σ-hole and the electronegative belt with the possible interactions that can occur involving these regions. Through modifications of the (i) halogen atom's polarizability,[39,40] (ii) hybridization of the group that the halogen atom is bonded to,[41,42] (iii) strength and number of the electron withdrawing (EWGs)[43–46] or donating groups (EDGs),[37] and (iv) location and distance of the substituents from the principle halogen atom,[37,43–45] the size and magnitude of the σ-hole ($V_{S,max}$) and the "belt" can be altered. An important point

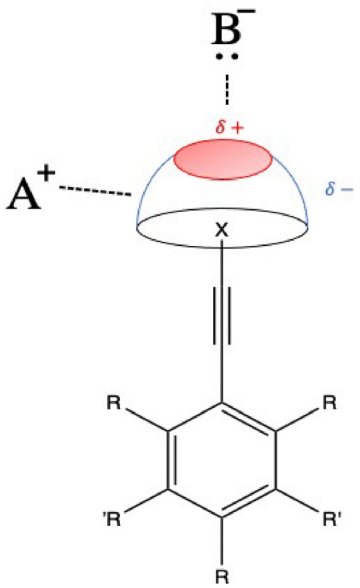

Fig. 1 Diagrammatic representation of the electropositive σ-hole (red) interacting with Lewis base B^-, electronegative belt (blue) interacting with Lewis acid A^+, and key geometrical parameters in an idealized RBAX-Lewis base model.

Department of Chemistry and Biochemistry, Baylor University, One Bear Place #97348, Waco, TX 76798-7348, USA. E-mail: kevin_shuford@baylor.edu

† Present address: Department of Chemistry, Southern Methodist University, Dallas, TX 75275, USA.

‡ Present address: Department of Chemistry and Physics, University of Tennessee Martin, 554 University Street, Martin, TN 38238, USA.

 This journal is © the Owner Societies 2025

Open Access Article. Published on 05 August 2025. Downloaded on 5/7/2026 3:16:31 AM. This article is licensed under a Creative Commons Attribution 3.0 Unported Licence.

to note is that the terms XB donors and XB acceptors used throughout this work are referring to the Lewis acids (*i.e.*, 1,2,3,4,5-pentafluoro(halo)ethynyl benzene (denoted as F_5BAX, where X = Br or I) and 1-(halo)ethynyl-3,5-dinitrobenzene (denoted as $(NO_2)_2$BAX, where X = Br or I)) and the Lewis bases (*i.e.*, 1,3,5-triazine (denoted as *s*-triazine or triazine), 1,3,5-triazine-2,4,6-trihydroxyl (denoted as isocyanuric acid), 1,3,5-triazine-2,4,6-trithiol (denoted as trithiolcyanuric acid), and 1,3,5-triazine-2,4,6-triphosphine (denoted as melPH_2)), respectively.

Graphitic carbon nitride (g-C_3N_4) is a promising semiconducting material widely studied for its photo/electrochemical properties, with photocatalysis as the primary focus.[47] These investigations have expanded to explore the optoelectronic characteristics and biocompatibility of g-C_3N_4 for application-based studies.[48] Graphitic carbon nitride is the most stable carbon nitride allotrope at mild conditions due the π-conjugation of the sp^2 hybridized carbon and nitrogen atoms.[49] This material is not only stable, it is a medium band gap semiconductor with good visible light response that assists in the photocatalytic applications and water splitting.[47,50–52] The band gap of g-C_3N_4 is known to be easily tunable, mainly through element interstitial or substitutional doping.[53–59] However, not many studies have focused on the intermolecular interactions that may take place between a g-C_3N_4 building block, with or without substitutions/dopants, and some other molecule. Sosa and co-workers[60] probed the NCIs formed between chlorinated or brominated cyanuric acid and melamine (*i.e.*, melamine/$(CACl)_{n=1-3}$ and melamine/$(CABr)_{n=1-3}$), and the authors discovered that the chlorine-containing complexes generally consist of only Cl···N XB interactions, whereas the bromine-containing complexes formed not only Br···N XB interactions but also belt···H hydrogen bonding interactions. Zou and coworkers[61] performed a study on the self-assembly of the high-pressured cyanuric chloride ($C_3N_3Cl_3$) crystal, where halogen bonding was found to be an effective non-covalent interaction to stabilize the crystal structure, and it exhibited a high compressibility and strong anisotropic compression. Bromine- and iodine-containing XB donors have been reported to interact with g-C_3N_4 building blocks (melamine and heptazine), exhibiting not only XB interactions but also HB interactions from the amine substituents in the g-C_3N_4 building blocks with the negative potential of the "belt" region surrounding the iodine and bromine atoms.[27,38] Hence, these studies highlight the need for further investigation of non-covalent interactions involving monomeric g-C_3N_4 building blocks and their derivatives, with an eye toward potential applications.

Herein, we extend our previous work on g-C_3N_4 monomers[27,38] by substituting the amine groups (–NH_2) in melamine (*i.e.*, 1,3,5-triazine-2,4,6-triamine) for hydrogen (–H), hydroxyl (–OH), thiol (–SH), and phosphine (–PH_2) groups, and observing how these substitutions affect the strength of the halogen bonding interactions. To further show how strong the XB and additional interactions are, we incorporate local mode analysis into our calculations. The addition of a second (third) XB donor to the 1 : 1 (2 : 1) XB donor : acceptor complexes yields binding energies that increase by approximately 90%. Similar to our previous works[27,38] and the work with Sosa and coworkers,[60] there were additional intermolecular HBs in conjunction with the XB interactions in select complexes. The results obtained through bond critical point and pathway analyses show the additional interactions, and the additive nature of the binding energies is supported by local mode analysis, which illustrates the additivity through the local mode force constants. The complexes formed produce stable complexes driven by XB interactions that possess a binding energy on the order of a hydrogen bond (*i.e.*, ∼5 kcal mol^{-1}) or slightly greater. With the additive effects, these complexes can form even stronger materials. We anticipate the concepts of supplemental and additive interactions demonstrated in this study to build upon the foundations of future materials and crystal engineering research. For example, adding π–π stacking interactions and other van der Waals forces to the system will strengthen each complex, leading the overall material to become much stronger and more resistant. The improved stability and strength of the material that is provided by the addition of multiple XB donors per one XB acceptor may also offer enhancements to the photocatalytic properties of g-C_3N_4.

Computational details

The XB donors, acceptors, and corresponding complexes were fully geometry optimized to compute intrinsic binding energies (E_{bind}). These binding energies were corrected for basis set superposition error through the Boys–Bernardi counterpoise procedure.[62] Harmonic vibrational frequency computations were performed on each monomer and complex to confirm that each stationary point corresponds to a minimum (*i.e.*, n_i = 0) on the potential energy surface and to compute the complexation shifts associated with the C–X and C≡C frequencies that accompany XB formation. Quantification of the maximum values of electrostatic potential (ESP) associated with the σ-hole ($V_{S,max}$), was obtained through a subsequent series of bond critical point (BCP) and pathway analyses.[63–66] The identification and characterization of key intermolecular interactions present between the XB donors and acceptors was accomplished through extending the BCP and pathway analyses to the XB complexes. The direction and magnitude of electron density transfer ($\Delta\rho$) between the XB donors and acceptors upon complexation was assessed through full natural bond orbital (NBO) analysis.[67–74]

The Gaussian 16 software package was used to compute all geometry optimizations, vibrational frequency calculations, NBO analyses, and where applicable, the gradients and Hessians therein.[75] The global hybrid M06-2X[76] density functional theory was used in conjunction with a double-ζ quality correlation consistent basis set augmented with diffuse functions on all atoms[77–79] with a relativistic pseudopotential on the bromine and iodine centers (*i.e.*, aug-cc-pVDZ for period 1–3 atoms; aug-cc-pVDZ-PP for Br and I; denoted aVDZ-PP) for all computations.[80,81] This level of theory was selected based on

Open Access Article. Published on 05 August 2025. Downloaded on 5/7/2026 3:16:31 AM. This article is licensed under a Creative Commons Attribution 3.0 Unported Licence.

the extensive calibrations by Kozuch and Martin[82] and Bauzá *et al.*[83] The Multiwfn software package was used for BCP and pathway analysis results.[84] As suggested by Bader *et al.*, a total electron isodensity of 0.001 electrons per Bohr^3 was used for the construction of all ESP maps.[85] The generation of all figures was produced through Tachyon ray tracing libraries[86] available in the visual molecular dynamics visualization software.[87]

In select complexes, there are additional intermolecular forces that compete with the main XB interaction. The binding energy (E_{bind}) accounts for all of the possible interactions and electronic effects that take place in the complexes. Therefore, E_{bind} cannot be used to compare the strengths of the individual atom–atom interactions. However, the normal vibrational modes are encoded with the detailed electronic structure and chemical bond information. Hence, the associated force constants and bond-stretching frequencies are great indicators for the intrinsic bond strengths of the inter- and intramolecular interactions. This concept follows from the Badger rule,[88] which states that the strength of a bond correlates with the frequency and related force constant of its vibrational mode. However, although this rule works very well for diatomic molecules, the extension to polyatomic molecules is much more problematic. This is due to the fact that the vibrational modes of polyatomic molecules are delocalized due to mass or electronic coupling, preventing a direct correlation between the stretching force constants and the bond strength. Hence, the local vibrational signatures and their affiliation with the electronic binding energies and the associated bond strength orders (BSOn; eqn (1)) of the individual XB donors and complexes are taken into consideration. The bond strength order is defined as

$$\mathrm{BSO}n = a(k_n^a)^b \quad (1)$$

where the constants a and b (a = 0.693, b = 0.556) are calculated from

$$a = \frac{n_2}{\left(k_2^a\right)^b} \quad (2)$$

and

$$b = \ln(n_2/n_1)/\ln(k_2^a/k_1^a) \quad (3)$$

using two reference compounds, I_2 and I_3^-, with known k^a (k_1^a = 1.882 mDyn Å^{-1}, k_2^a = 0.651 mDyn Å^{-1}) and BSOn values (n_1 = 1.0, n_2 = 0.5), respectively.[89] The constraint put on eqn (1) is that the BSOn value has to be zero when the force constant is zero.[89–91] This analysis has been applied successfully for the characterization of covalent[92–95] and non-covalent bonds such as XBs,[89,91,96,97] ChBs,[98,99] HBs,[100–104] and many more. Here we employ the M06-2X/aVDZ-PP Hessians alongside the local mode analysis code (LModeA) developed by Kraka and coworkers[105] through the inspiration of Konkoli and Cremer.[106] An extensive review of local vibrational theory is provided by Kraka *et al.*[90,107,108]

Results and discussion

In our previous study,[27] we saw that melamine and heptazine g-C_3N_4 building blocks formed rather strong XB complexes. This was further elaborated upon by looking into the vibrational spectroscopy of the complexes that indicated XBs were the main driver of the complexation, but weak HB interactions also contributed to the formation of strong, stable complexes.[38] Herein we extend these studies to obtain a more fundamental understanding of NCIs in these complexes by examining the effects that different substituents may generate. Specifically, the amine groups bound to the triazine ring were substituted with H, OH, SH, and PH_2 functional groups, as seen in Fig. 2 (right side). There are three potential locations on the acceptors where the XB donors can possibly bind (ring N sites, blue $\delta-$ ESP), with 1 to 6 hydrogen atoms that can potentially assist in the XB complex formation.

The XB donors that are featured throughout this work (*i.e.*, F_5BAX and $(NO_2)_2$BAX, where X = Br or I) are displayed in Fig. 2, and the values of $V_{S,max}$ as well as the C–X and C≡C local stretch force constants are presented in Table 1. As seen in our previous paper upon performing local mode analysis on XB-g-C_3N_4 systems,[38] the C≡C stretch local force constant has a very good correlation to the $V_{S,max}$, and the C–X stretch local force constant has a slightly worse correlation. Since the local force constants are a direct comparison to bond strength, these values will be used throughout when examining the trends occurring upon complexation.

1 : 1 donor–acceptor complexes

Fig. 3 depicts the geometry-optimized structures with corresponding BCP and pathway analyses for the global minimum

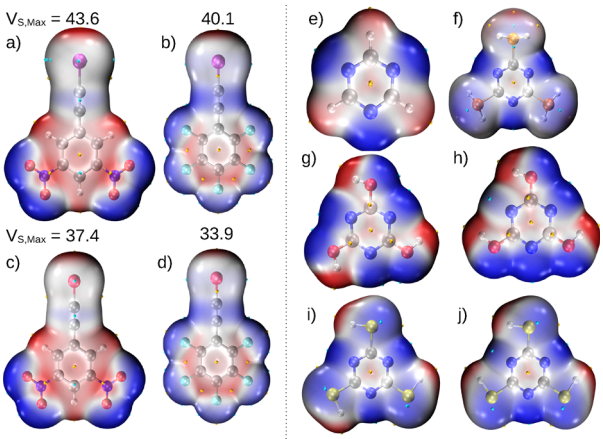

Fig. 2 Electrostatic potential (ESP) maps of the fully optimized geometries of the isolated halogen bond donors (left; (a) is $(NO_2)_2$BAI, (b) is F_5BAI, (c) is $(NO_2)_2$BABr, and (d) is F_5BABr) and acceptors (right; (e) is triazine, (f) is melPH_2, (g) is global minimum of isocyanuric acid, (h) is the C_s symmetry higher energy conformer of isocyanuric acid, (i) is global minimum of trithiolcyanuric acid, and (j) is the C_s symmetry higher energy conformer of trithiolcyanuric acid) at the M06-2X/aVDZ-PP level of theory. The $V_{S,max}$ values of the donors correspond to the magnitudes of the σ-hole in kcal mol^{-1}. The $\delta+$ regions of the ESP are shaded red, and the $\delta-$ regions are shaded blue.

 This journal is © the Owner Societies 2025

Open Access Article. Published on 05 August 2025. Downloaded on 5/7/2026 3:16:31 AM.
This article is licensed under a Creative Commons Attribution 3.0 Unported Licence.

Table 1 Magnitude of the σ-hole ($V_{S,max}$ in kcal mol^{-1}) and local C–X and C≡C stretching force constants (k^a_{C-X} and $k^a_{C\equiv C}$ in mDyn Å^{-1}) of the isolated XB donors at the M06-2X/aVDZ-PP level of theory

Donor	$V_{S,max}$	k^a_{C-X}	$k^a_{C\equiv C}$
F_5BABr	33.9	4.552	17.264
$(NO_2)_2$BABr	37.4	4.579	17.194
F_5BAI	40.1	3.607	17.060
$(NO_2)_2$BAI	43.6	3.594	16.993

conformers of the 1:1 XB donor:acceptor complexes (*i.e.*, F_5BAX–triazine, $(NO_2)_2$BAX–triazine, F_5BAX–isocyanuric acid, $(NO_2)_2$BAX–isocyanuric acid, F_5BAX–trithiolcyanuric acid, $(NO_2)_2$BAX–trithiolcyanuric acid, F_5BAX–melPH$_2$, and $(NO_2)_2$BAX–melPH$_2$, where X = I, Br). Local minima corresponding to higher energy conformers can be found in the SI as complexes **3.1–3.4**, **5.1–7.4**, and **9.1–11.4** (Schemes S1–S3). The electronic binding energy (E_{bind}), shifts in the vibrational frequencies, X···N interaction distance (R_{X-N}), local adiabatic force constant for the X···N interaction (k^a_{X-N}), average H···X interaction distance (R^{avg}_{H-X}), average local adiabatic force constant for H···X interaction (k^a_{H-X}), bond strength order (BSOn) of the X···N and H···X interactions, and the magnitude of electron density ($\Delta\rho$) transferred from the Lewis base to Lewis acid for each corresponding global minimum XB complex are shown in Table 2.

Our previous work with melamine and heptazine showed that the 1:1 F_5BAX– and $(NO_2)_2$BAX–melamine (X = Br, I) complexes conform to a C_{2v} point group symmetry, whereas the heptazine containing complexes have a C_s point group symmetry.[27] Substituting the amine groups in melamine for PH_2 (complexes **2.1–2.4**) or thiol functional groups (complexes **8.1–8.4**) results in a C_1 point group symmetry (Fig. 3). The C_1 symmetries are a result of the complexes forming nonplanar structures with the XB donors coming from slightly above or below the XB acceptors yielding a slight cant with respect to the XB acceptor. Complexes **4.1–4.4**, where the amine groups in melamine are substituted for hydroxyl groups, have a point group symmetry of C_s (Fig. 3). The angle of the XB interaction is slightly influenced by the hydrogen atoms in the hydroxyl substituents, causing a small deviation from the typical 180° interaction angle. However, the XB angle only has a max deviation of 6°, remaining mostly linear. Complexes **1.1** and **1.2** (Fig. 3) also form structures where the XB interaction angle is not completely linear, resulting in a point group symmetry of C_s. Complexes **1.3** and **1.4** (Fig. 3) produce structures with linear C–X···N interaction angles, but the XB donor has a slight cant with respect to the triazine acceptor, thus inducing a C_2 point group symmetry. These results are a reoccurring theme among all the XB complexes shown throughout this study.

In our previous study with melamine and heptazine, an appreciable difference of ∼3 kcal mol^{-1} in the binding energy was observed between the XB complexes containing bromine and iodine.[27] The differences in the binding energies ascertained between the bromine and iodine containing complexes studied in this work are ∼1–2 kcal mol^{-1} (Table 2). This observed change in the binding energies between XB systems can be partly attributed to the fact that the additional hydrogen bonding interactions from the amine groups were stronger and more prevalent in the previous study than in the complexes shown here. This is backed up by the local force constants (k^a)

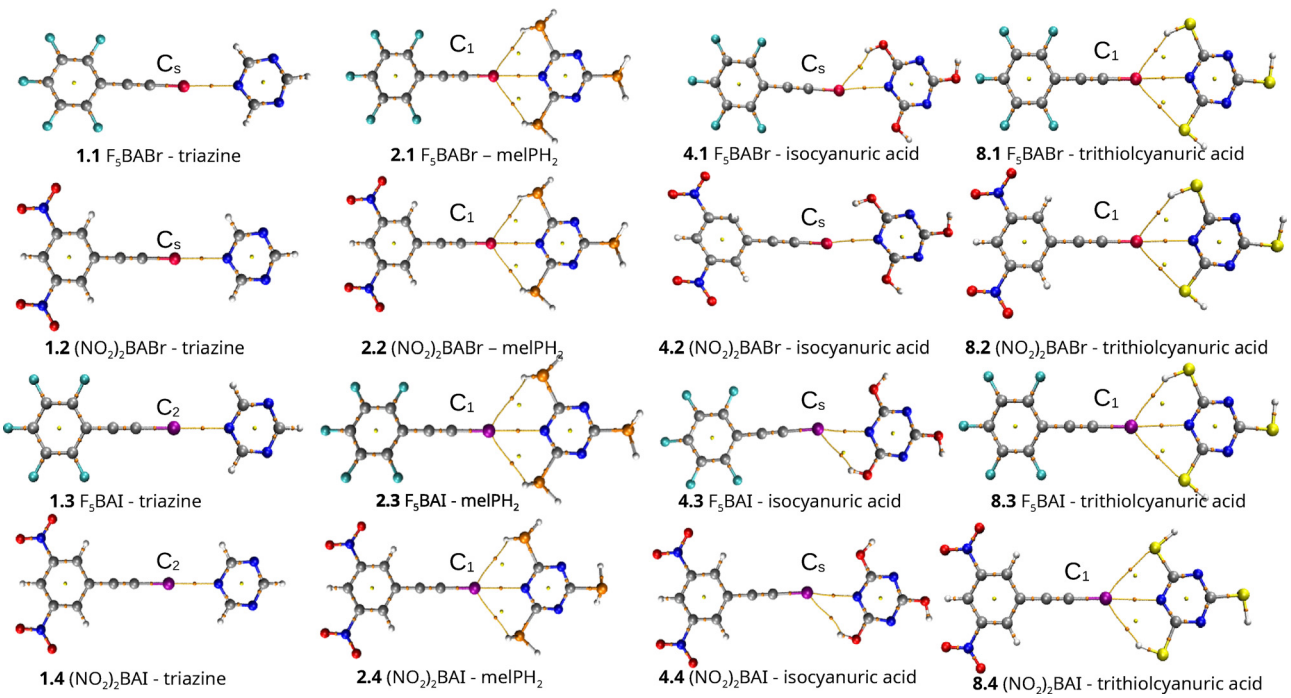

Fig. 3 Fully optimized geometries with the corresponding point group symmetries, bond critical points (orange spheres) and pathways (orange lines) of the 1:1 XB donor:acceptor dimer complexes at the M06-2X/aVDZ-PP level of theory.

Open Access Article. Published on 05 August 2025. Downloaded on 5/7/2026 3:16:31 AM. This article is licensed under a Creative Commons Attribution 3.0 Unported Licence.

Table 2 Halogen bond lengths (R_{X-N}; Å), local mode force constant of the halogen bond (k^a_{X-N}; mDyn Å^{-1}), bond strength order of the halogen bond (BSOn_{X-N}), average bond length of the supplemental hydrogen bonds (R^{avg}_{H-X}; Å), average local mode force constant of the supplemental hydrogen bonds (k^a_{H-X}; mDyn Å^{-1}), average bond strength order of the supplemental hydrogen bonds (BSOn_{H-X}), complexation shifts in the C–X and C≡C vibrational frequencies ($\Delta\nu_{C-X}$ and $\Delta\nu_{C\equiv C}$; cm^{-1}), magnitude of electron density transfer upon complexation ($\Delta\rho$; millielectrons), and electronic binding energy (E_{bind}; kcal mol^{-1}) of each 1 : 1 donor : acceptor XB complex at the M06-2X/aVDZ-PP level of theory

XB donor	R_{X-N}	k^a_{X-N}	BSOn_{X-N}	R^{avg}_{H-X}	k^a_{H-X}	BSOn_{H-X}	$\Delta\nu_{C\equiv C}$	$\Delta\nu_{C-X}$	$\Delta\rho$	E_{bind}
With a triazine XB acceptor										
F_5BABr	2.91	0.158	0.198	3.71	—	—	−7	0	0.018	−4.56
$(NO_2)_2$BABr	2.91	0.160	0.200	3.71	—	—	−8	−2	0.019	−4.70
F_5BAI	2.94	0.182	0.218	3.73	—	—	−9	−3	0.030	−6.39
$(NO_2)_2$BAI	2.93	0.187	0.221	3.72	—	—	−9	−5	0.032	−6.57
With a isocyanuric acid XB acceptor										
F_5BABr	2.92	0.167	0.206	2.84	0.020	0.051	−5	0	0.015	−4.99
$(NO_2)_2$BABr	2.91	0.168	0.206	2.89	0.016	0.044	−6	−2	0.016	−5.03
F_5BAI	2.96	0.187	0.221	2.95	0.044	0.086	−7	−3	0.025	−6.87
$(NO_2)_2$BAI	2.95	0.191	0.225	2.97	0.041	0.082	−8	−4	0.027	−6.96
With a trithiolcyanuric acid XB acceptor										
F_5BABr	2.96	0.165	0.204	2.85	0.068	0.114	−5	0	0.009	−4.88
$(NO_2)_2$BABr	2.95	0.167	0.206	2.86	0.074	0.121	−6	0	0.010	−4.92
F_5BAI	3.03	0.178	0.214	2.92	0.100	0.147	−7	−2	0.014	−6.43
$(NO_2)_2$BAI	3.02	0.178	0.214	2.92	0.102	0.149	−7	−3	0.016	−6.50
With a melPH_2 XB acceptor										
F_5BABr	2.94	0.162	0.202	3.18	0.039	0.079	−7	2	0.015	−5.29
$(NO_2)_2$BABr	2.94	0.164	0.203	3.19	0.040	0.080	−8	−1	0.016	−5.39
F_5BAI	3.00	0.168	0.206	3.29	0.034	0.072	−9	−4	0.023	−7.03
$(NO_2)_2$BAI	2.99	0.164	0.203	3.30	0.014	0.041	−9	−2	0.025	−7.16

and bond strength orders (BSOn) provided (Table 2). As seen in the local mode analysis performed in our previous work,[38] the cumulative strength of the hydrogen bonds formed are relatively strong, falling in the intermediate strength category of bond strength order ($0.15 < \text{BSO}n < 0.30$). However, in these complexes, the average strength of each hydrogen bond in the XB complexes are relatively weak (BSOn < 0.15), with complexes **8.3**, **8.4** (Table 2), **10.3**, and **10.4** (Scheme S2) on the borderline between weak and intermediate HBs (Table S2). This trend remains even when there is more than one hydrogen atom interacting with the same XB donor (Table 2 and Tables S1–S3). It is also important to note that the additional HB interactions may or may not occur based on where the XB donor is interacting with the XB acceptor. For instance, consider complexes **2.1–3.4** (Fig. 3 and Scheme S3). Complexes **3.1–3.4** do not experience any HB interactions due to the distance separating the halogen and hydrogen atoms. However, the XB donors do have an interaction with the P atoms in the PH_2 groups in complexes **3.3** and **3.4**, as seen by the pathway analyses in Scheme S3. There also exist complexes, such as complexes **4.2** (Fig. 3), **5.1–6.2**, and **6.4** (Scheme S1), where dispersion interactions between the hydrogen atoms in the substituents on the triazine ring and the halogen atom of the XB donor exists; however, these interactions are too weak to be shown through the BCP and pathway analyses. However, in complexes **2.1–2.4**, the two hydrogen atoms closest to the XB donor interact with the electronegative belt encompassing the halogen atom, thus forming hydrogen bonds as provided by BCP and pathway analyses (Fig. 3) with support from local mode analyses (Table 2 and Table S3). However, this does not necessarily equate to a larger binding energy, rather the polarization effects of the σ-hole (∼10 kcal mol^{-1} difference between iodine and bromine XB donors) play a larger role in the majority of the XB complexes, with complexes **5.1–5.4** (Scheme S1) and **9.1–9.4** (Scheme S2) being the exceptions.

The identity of the electron donating groups (EDGs) bound to the triazine backbone is also a key factor in why these binding energies have such a small difference between the iodine- and bromine containing complexes. The –H, –OH, –SH, and –PH_2 groups are much weaker EDGs compared to –NH_2 in melamine and heptazine. This leads to less back-donation of electrons into the π-system, which ultimately leads to less electron density accumulating on the nitrogen atoms in the triazine ring. This was similarly seen by Bankiewicz and Palusiak in their work with halogen bonding in diaminopyridine and pyridine with EDG substituents added in the XB acceptor systems.[109] Ranking the substituents in terms of electron-donating capacity, the –NH_2 group would be ranked first, followed by the –OH, and then the –PH_2 and –SH groups. Table 2 shows that the isocyanuric acid acceptors have a slightly larger BSO$n_{X\cdots N}$ compared to the trithiolcyanuric acid and melPH_2 acceptors, and the magnitude of charge transferred from the XB acceptor to the XB donor is roughly equivalent for isocyanuric acid and melPH_2, with both being significantly more than trithiolcyanuric acid. This suggests the isocyanuric acid acceptors would have the strongest binding energy, but these acceptors end up second behind melPH_2 due to secondary interactions. The BSO$n_{H\cdots X}$ values and number of HBs assist in explaining why the melPH_2 acceptors have the strongest binding energy. The BSO$n_{H\cdots X}$ in the melPH_2 acceptors is

 This journal is © the Owner Societies 2025

Open Access Article. Published on 05 August 2025. Downloaded on 5/7/2026 3:16:31 AM.
This article is licensed under a Creative Commons Attribution 3.0 Unported Licence.

either larger than the isocyanuric acid acceptors or effectively larger upon considering two HBs form (see **2.1–2.4** in Fig. 3). Moreover, the BSO$n_{H\cdots X}$ values in the melPH$_2$ acceptors are effectively larger than or comparable to trithiolcyanuranic acid for most donors, given the latter has a single HB and a competing XB (see **8.1–8.4** in Fig. 3). This shows that hydrogen bonding is generally strongest in the melPH$_2$ complexes, followed by trithiolcyanuranic acid and then isocyanuric acid complexes. Complexes with additional or stronger HBs facilitate more electron density being transferred back into the triazine ring of the acceptor, which can enhance interactions with the halogen in the donor and increase binding. The ESP maps in Fig. 2 also show wide areas of negative potential in the isocyanuric and thiolcyanuric acid acceptor, which can also interact with the electronegative belt around the halogen atom in the XB donor. This prevents the fully attractive interaction between XB donor and acceptor, which in turn reduces the interaction strength.

Although the additional HB interactions are relatively weak, the XB interactions on the other hand fall into the intermediate category ($0.15 < \mathrm{BSO}n < 0.30$) regardless of where the halogen atom is interacting with the XB acceptor. This is also backed by the change in the frequency of the C$\equiv$C stretch ($\Delta\nu_{C\equiv C} \approx -7$ to -12 cm^{-1}), as these frequencies are the most reliable modes to determine XB formation and strength compared to the C–X stretch.[38] Unlike the melamine and heptazine complexes where there was a red-shift (*i.e.*, shift to lower energy) in C–X and C$\equiv$C stretches (*i.e.*, $\Delta\nu_{C-X} < 0$ and $\Delta\nu_{C\equiv C} < 0$) for all XB donors, a few of the bromine-containing complexes did not have a C–X stretch frequency shift ($\Delta\nu_{C-X} = 0$) and a couple very slightly blue-shifted (*i.e.*, shift to higher energy, $\Delta\nu_{C-X} > 0$). A possible reason for the C–X bond stretches in the 1 : 1 F_5BABr : XB acceptor complexes slightly blue-shifting or not shifting at all could potentially be explained by the C–X bond local force constant having a much smaller change upon complexation (Δk^a_{C-X}) when compared to the complexes with the other XB donors (Tables S8–S11). The smaller change in Δk^a_{C-X} can be understood by the magnitude of charge transferred from the XB acceptor to XB donor ($\Delta\rho$) that is smaller compared to the other complexes (Table 2). This means that there is a smaller influx of electron density moving into the C–X bond in the F_5BABr:XB acceptor complexes than the other complexes. The C$\equiv$C stretch frequency was red-shifted for all complexes.

2 : 1 and 3 : 1 donor–acceptor complexes

A propagation of the 1 : 1 XB donor : acceptor complexes was carried out to form the 2 : 1 XB donor : acceptor complexes shown in Fig. 4. Each fully optimized geometry displayed in the figure represents a minimum on the M06-2X/aVDZ-PP potential energy surface with BCP and pathway analyses accounted for. As with the majority of the 1 : 1 complexes, the 2 : 1 complexes conform to either a C_1 or C_s symmetry (Fig. 4), with the sole exception of complex **12.4** conforming to a point group of C_{2v}. The C–X$\cdots$N bond angle is approximately linear, with a deviation of at most 9°, agreeing with the bond directionality of halogen bonds.

Table 3 shows that X$\cdots$N interaction is slightly weakened for each individual XB formed; however, the sum of the X$\cdots$N interactions attributes to the increase in E_{bind}. These points provide a reasonable explanation for the >90% additivity of the interactions yet not being completely additive. The variation of additivity ranging between 90% and 98% is due to the fact that the additional HB interactions do not follow this trend. In some complexes, the HB interactions increase in strength with each increasing XB donor (isocyanuric acceptor in Tables 2 and 3), while other complexes see a decrease in HB strength with each increasing XB donor (thiolcyanuric acceptor in Tables 2 and 3). The X$\cdots$N interaction decreases in strength with the addition of

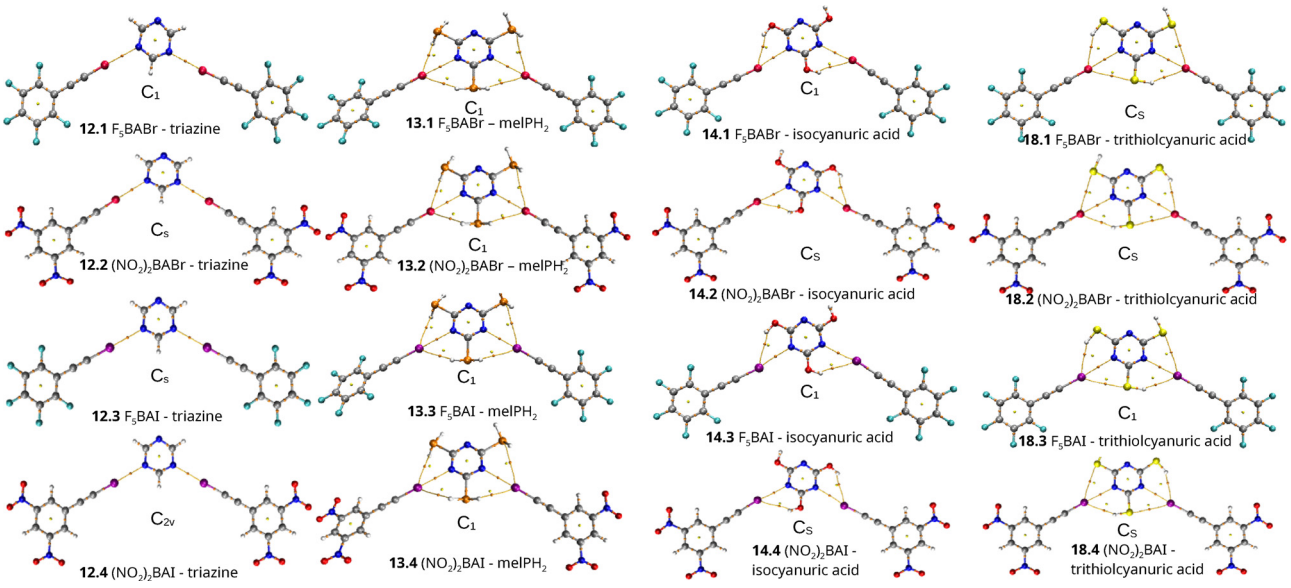

Fig. 4 Fully optimized geometries with the corresponding point group symmetries, bond critical points (orange spheres) and pathways (orange lines) of the 2 : 1 XB donor : acceptor trimer complexes at the M06-2X/aVDZ-PP level of theory.

Open Access Article. Published on 05 August 2025. Downloaded on 5/7/2026 3:16:31 AM. This article is licensed under a Creative Commons Attribution 3.0 Unported Licence.

Table 3 Halogen bond lengths (R_{X-N}; Å), local mode force constant of the halogen bond (k^a_{X-N}; mDyn Å^{-1}), bond strength order of the halogen bond (BSOn_{X-N}), average bond length of the supplemental hydrogen bonds (R^{avg}_{H-X}; Å), average local mode force constant of the supplemental hydrogen bonds (k^a_{H-X}; mDyn Å^{-1}), average bond strength order of the supplemental hydrogen bonds (BSOn_{H-X}), complexation shifts in the C–X and C≡C vibrational frequencies ($\Delta\nu_{C-X}$ and $\Delta\nu_{C\equiv C}$; cm^{-1}), magnitude of electron density transfer upon complexation ($\Delta\rho$; millielectrons), and electronic binding energy (E_{bind}; kcal mol^{-1}) of each 2 : 1 donor : acceptor XB complex at the M06-2X/aVDZ-PP level of theory

XB donor	R_{X-N}	k^a_{X-N}	BSOn_{X-N}	R^{avg}_{H-X}	k^a_{H-X}	BSOn_{H-X}	$\Delta\nu_{C\equiv C}$	$\Delta\nu_{C-X}$	$\Delta\rho$	E_{bind}
With a triazine XB acceptor										
F_5BABr	2.93	0.151	0.193	3.63	—	—	−6(−7)	0(0)	0.032	−8.75
$(NO_2)_2$BABr	2.93	0.154	0.195	3.71	—	—	−7(−7)	−1(−1)	0.033	−8.78
F_5BAI	2.97	0.166	0.205	3.75	—	—	−7(−8)	−2(−3)	0.052	−12.00
$(NO_2)_2$BAI	2.96	0.167	0.206	3.75	—	—	−7(−7)	−4(−4)	0.054	−12.06
With a isocyanuric acid XB acceptor										
F_5BABr	2.93	0.162	0.202	2.81	0.033	0.071	−4(−4)	0(0)	0.025	−9.78
$(NO_2)_2$BABr	2.93	0.165	0.204	2.85	0.026	0.061	−5(−5)	−2(−2)	0.028	−9.65
F_5BAI	2.98	0.179	0.215	2.93	0.045	0.087	−6(−6)	−2(−2)	0.042	−13.28
$(NO_2)_2$BAI	2.97	0.182	0.217	2.95	0.044	0.086	−6(−6)	−4(−4)	0.045	−13.18
With a trithiolcyanuric acid XB acceptor										
F_5BABr	2.97	0.159	0.199	2.84	0.064	0.110	−5(−5)	0(1)	0.016	−9.57
$(NO_2)_2$BABr	2.97	0.161	0.201	2.85	0.068	0.114	−5(−5)	0(−1)	0.017	−9.45
F_5BAI	3.06	0.172	0.209	2.91	0.098	0.145	−5(−6)	−1(−2)	0.022	−12.44
$(NO_2)_2$BAI	3.05	0.171	0.209	2.91	0.099	0.146	−5(−5)	−3(−2)	0.024	−12.33
With a melPH$_2$ XB acceptor										
F_5BABr	2.95	0.161	0.200	3.24	0.041	0.082	−6(−6)	0(−1)	0.027	−10.45
$(NO_2)_2$BABr	2.94	0.160	0.200	3.25	0.031	0.068	−7(−7)	−1(−1)	0.028	−10.46
F_5BAI	3.02	0.170	0.208	3.33	0.048	0.091	−7(−7)	−2(−3)	0.040	−13.74
$(NO_2)_2$BAI	3.01	0.170	0.208	3.34	0.033	0.071	−7(−7)	−3(−5)	0.042	−13.77

a second XB donor for all complexes with the exception of complexes **13.3**, **13.4** (Tables 2, 3 and Table S3), **19.1**, **21.3**, and **21.4** (Tables S2 and S5). The C–X and C≡C bonds, on the other hand, increase in strength with each additional XB donor in the complex, while the average C–X and C≡C bond strengths are weaker than the XB donor monomers, as observed by the negative values for Δk^a_{C-X} in Tables S8–S11. This is due to the decrease in electron density being transferred to each individual XB donor in the complex relative to the original amount amount transferred in the 1 : 1 complexes. The decrease in electron density transferred to individual units of XB donor effectively decreases the electron–electron repulsion occurring between nuclei, thus allowing for stronger C–X and C≡C bonds.

Another way to analyze the cooperativity is by looking at the average synergy of the complex. The average synergy (eqn (4), adapted for these non-chain systems), which is a measure that quantifies cooperativity in complexes,[110] is given as:

$$\Delta E^{complex}_{syn} = \frac{E^{complex}_{bind}}{n_{donor}} - E^{dimer}_{bind}. \quad (4)$$

Here the average synergy of the complex is the difference between the binding energy of the complex ($E^{complex}_{bind}$) divided by the number of XB donors present (n_{donor}), and the binding energy of the 1 : 1 XB donor : acceptor dimer (E^{dimer}_{bind}). Table 4 shows that the average synergy of each trimer and tetramer are positive, thus showing that the interactions present are not completely cooperative (additive) in nature. In addition, the XB complexes containing iodine have a more positive synergy compared to the bromine containing complexes. This shows that the iodine-containing complexes have a lesser degree of cooperativity compared to the bromine derivatives. It is also observed that the F_5BAX donors are more cooperative (have less positive synergy) compared to the $(NO_2)_2$BAX donors in the trimeric and tetrameric complexes (Table 4). Therefore, the F_5BAX donors provide more stabilization to the 2 : 1 and

Table 4 Binding energy of the dimer, trimer, and tetramer (E^{dimer}_{bind}, E^{trimer}_{bind}, and $E^{tetramer}_{bind}$; kcal mol^{-1}), and average synergy for the trimer and tetramer systems (ΔE^{trimer}_{syn} and $\Delta E^{tetramer}_{syn}$; kcal mol^{-1}) at the M06-2X/aVDZ-PP level of theory

XB donor	E^{dimer}_{bind}	E^{trimer}_{bind}	$E^{tetramer}_{bind}$	ΔE^{trimer}_{syn}	$\Delta E^{tetramer}_{syn}$
With a triazine XB acceptor					
F_5BABr	−4.56	−8.75	−12.60	0.19	0.36
$(NO_2)_2$BABr	−4.70	−8.78	−12.34	0.31	0.58
F_5BAI	−6.39	−12.00	−17.00	0.39	0.72
$(NO_2)_2$BAI	−6.57	−12.06	−16.72	0.54	0.99
With a isocyanuric acid XB acceptor					
F_5BABr	−4.99	−9.78	−14.41	0.10	0.18
$(NO_2)_2$BABr	−5.03	−9.65	−13.92	0.21	0.39
F_5BAI	−6.87	−13.28	−19.37	0.23	0.41
$(NO_2)_2$BAI	−6.96	−13.18	−18.87	0.37	0.67
With a trithiolcyanuric acid XB acceptor					
F_5BABr	−4.88	−9.57	−14.07	0.10	0.19
$(NO_2)_2$BABr	−4.92	−9.45	−13.64	0.20	0.38
F_5BAI	−6.43	−12.44	−18.11	0.21	0.39
$(NO_2)_2$BAI	−6.50	−12.33	−17.63	0.33	0.62
With a melPH$_2$ XB acceptor					
F_5BABr	−5.29	−10.45	−15.15	0.21	0.39
$(NO_2)_2$BABr	−5.39	−10.46	−14.84	0.36	0.64
F_5BAI	−7.03	−13.74	−19.60	0.42	0.76
$(NO_2)_2$BAI	−7.16	−13.77	−19.26	0.58	1.05

 This journal is © the Owner Societies 2025

Open Access Article. Published on 05 August 2025. Downloaded on 5/7/2026 3:16:31 AM.
This article is licensed under a Creative Commons Attribution 3.0 Unported Licence.

3 : 1 donor : acceptor complexes compared to the $(NO_2)_2$BAX counterparts.

Our observations of the XB complexes not being cooperative in nature differs from some reports in the literature on linear and cyclic XB complexes. Yan *et al.* found that linear chains of 4-bromopyridine and 1-bromo-1*H*-imidazole display cooperativity of the energy that increases with each additional XB donor added into the chain.[111] They also found the average halogen bond strength increases in magnitude with each increase in XB donor site in multiply halogen bonded systems. Parra observed cooperativity in a cyclic network constructed from IF molecules with the number of molecules being greater than three.[112] These two studies showcase the cooperative nature of halogen bonds when the halogen containing molecule is used as an XB donor and acceptor. However, Bedeković *et al.* and Côté *et al.* found that when multiple XB acceptors interact with a single XB donor, the addition of each XB acceptor is anticooperative in nature, meaning that the binding energy of each additional interaction is not 100% additive.[113,114] This study and our previous work[27] exhibit that the reverse is true as well

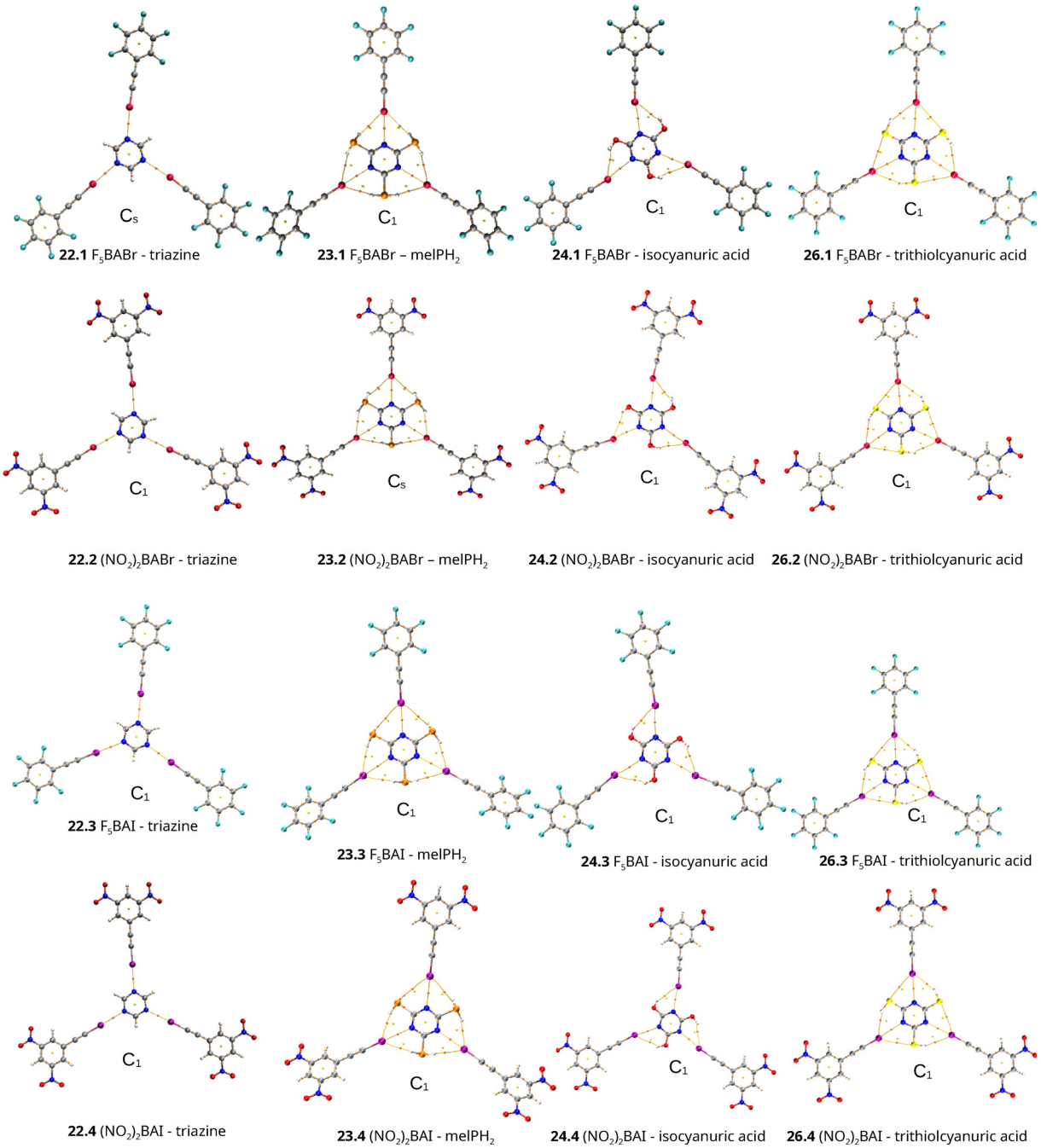

Fig. 5 Fully optimized geometries with the corresponding point group symmetries, bond critical points (orange spheres) and pathways (orange lines) of the 3 : 1 XB donor : acceptor tetramer complexes at the M06-2X/aVDZ-PP level of theory.

Open Access Article. Published on 05 August 2025. Downloaded on 5/7/2026 3:16:31 AM.
This article is licensed under a Creative Commons Attribution 3.0 Unported Licence.

(*i.e.*, multiple XB donors per one XB acceptor display similar behavior).

The addition of an extra XB donor in the complexes shows that the binding energy is less reliant on the magnitude of the σ-hole. As seen in Table 3, the F_5BAX donors are forming slightly stronger complexes compared to the $(NO_2)_2$BAX donors. The exceptions to this are complexes **17.1–17.4** (Scheme S4), **20.3–20.4** and **21.1–21.4** (Scheme S5), and **13.1–13.4** (Fig. 4) shown in Tables S10, S11, and Table 3, respectively. We observe that there is a stronger X···N interaction in the $(NO_2)_2$BAX donors compared to the F_5BAX donors, with the X···N and H···X bond lengths diverging by at most 0.01 Å between complexes. However, the complexes where the F_5BAX donors have the strongest binding energy, the X···N interactions have a similar magnitude of strength (as observed from the BSO*n*) between complexes, with the X···N bond lengths being similar to the $(NO_2)_2$BAX complexes and the H···X bond lengths being shorter (outside the 0.01 Å divergence) in the F_5BAX complexes when compared to the $(NO_2)_2$BAX complexes. This allows the H···X interaction in the F_5BAX complexes to be as strong if not stronger than the H···X interactions in the $(NO_2)_2$BAX complexes. These trends show that although the X···N interaction is the dominant interaction and largest contributor to the binding energy, the supplemental HBs are determining factors in the stability of the complexes as well.

The inclusion of a third XB donor completes the saturation of the XB acceptor, forming the tetrameric structures presented in Fig. 5. The structural and electronic data for these complexes can be viewed in Table 5 and Tables S6, S7. The individual X···N interactions slightly weaken further when an additional XB donor is added to a 2 : 1 donor : acceptor complex (Table 5 and Tables S6, S7). However, the contribution of each donor : acceptor interaction bestows approximately a 90% increase to the binding energy of the complex, or in terms of synergy, the 3 : 1 donor : acceptor complexes are between 0.2 and 1.0 kcal mol^{-1} short of being 100% cooperative (Table 4). Table 4 also shows that the synergy becomes more positive when the number of XB donors per acceptor increases. In other words, the percent additivity decreases when moving from a trimer to tetramer donor:acceptor complexes. In addition, the difference between the binding energy of the 3 : 1 donor : acceptor complexes between the F_5BAX and $(NO_2)_2$BAX donors has become much larger when compared to the 2 : 1 donor : acceptor complexes (Tables 3–5). This shows that the value of the $V_{S,max}$ of the XB donor (Fig. 2) matters less when the size of the complexes increase.

Another interesting observation made in the 3 : 1 donor : acceptor complexes through local mode analysis is that the triazine acceptor is showing small H···X interactions in the complexes, which were not present in the 2 : 1 or 1 : 1 donor : acceptor complexes. The local mode analysis results, supplemented with NBO, suggests that the electron density transferred to the XB donors and the lone pairs of the halogen atom donating electron density to the adjacent nitrogen atoms in the triazine ring is large enough to constitute the hydrogen atoms forming stronger dispersion interactions with the electronegative belt around the halogen atoms. However, these dispersion interactions are still considerably weak and are not strong enough to be considered hydrogen bond interactions. Hence, the BCP and pathway analyses (Fig. 5) do not show the

Table 5 Halogen bond lengths (R_{X-N}; Å), local mode force constant of the halogen bond (k^a_{X-N}; mDyn Å^{-1}), bond strength order of the halogen bond (BSOn_{X-N}), average bond length of the supplemental hydrogen bonds (R^{avg}_{H-X}; Å), average local mode force constant of the supplemental hydrogen bonds (k^a_{H-X}; mDyn Å^{-1}), average bond strength order of the supplemental hydrogen bonds (BSOn_{H-X}), complexation shifts in the C–X and C≡C vibrational frequencies ($\Delta\nu_{C-X}$ and $\Delta\nu_{C\equiv C}$; cm^{-1}), magnitude of electron density transfer upon complexation ($\Delta\rho$; millielectrons), and electronic binding energy (E_{bind}; kcal mol^{-1}) of each 3 : 1 donor : acceptor XB complex at the M06-2X/aVDZ-PP level of theory

XB donor	R^{avg}_{X-N}	k^a_{X-N}	BSOn_{X-N}	R^{avg}_{H-X}	k^a_{H-X}	BSOn_{H-X}	$\Delta\nu_{C\equiv C}$	$\Delta\nu_{C-X}$	$\Delta\rho$	E_{bind}
With a triazine XB acceptor										
F_5BABr	2.94	0.146	0.188	3.70	0.010	0.032	−5(−5)	0(0)	0.043	−12.60
$(NO_2)_2$BABr	2.95	0.145	0.187	3.73	0.008	0.029	−1(−1)	−5(−5)	0.044	−12.34
F_5BAI	2.99	0.160	0.200	3.78	0.007	0.026	−6(−6)	−1(−2)	0.069	−17.00
$(NO_2)_2$BAI	2.99	0.158	0.199	3.78	0.006	0.023	−5(−5)	−3(−3)	0.070	−16.72
With a isocyanuric acid XB acceptor										
F_5BABr	2.94	0.154	0.195	2.78	0.033	0.072	−3(−4)	0(0)	0.032	−14.41
$(NO_2)_2$BABr	2.94	0.159	0.199	2.81	0.034	0.072	−4(−5)	−2(0)	0.035	−13.92
F_5BAI	2.99	0.175	0.212	2.91	0.054	0.099	−5(−5)	−2(−1)	0.053	−19.37
$(NO_2)_2$BAI	2.99	0.175	0.212	2.92	0.049	0.093	−4(−4)	−3(−4)	0.056	−18.87
With a trithiolcyanuric acid XB acceptor										
F_5BABr	2.98	0.160	0.200	2.83	0.070	0.117	−4(−4)	1(2)	0.020	−14.07
$(NO_2)_2$BABr	2.98	0.163	0.202	2.84	0.078	0.125	−5(−4)	0(0)	0.021	−13.64
F_5BAI	3.07	0.167	0.206	2.89	0.099	0.146	−4(−5)	−1(−2)	0.025	−18.11
$(NO_2)_2$BAI	3.07	0.164	0.204	2.90	0.097	0.145	−4(−4)	−1(−2)	0.027	−17.63
With a melPH$_2$ XB acceptor										
F_5BABr	2.96	0.156	0.197	3.17	0.041	0.082	−5(−5)	0(−1)	0.035	−15.15
$(NO_2)_2$BABr	2.96	0.155	0.196	3.18	0.039	0.080	−5(−6)	−1(−1)	0.036	−14.84
F_5BAI	3.05	0.158	0.199	3.26	0.030	0.067	−6(−6)	−1(−2)	0.051	−19.60
$(NO_2)_2$BAI	3.05	0.161	0.201	3.27	0.039	0.080	−5(−5)	−4(−6)	0.053	−19.26

 This journal is © the Owner Societies 2025

Open Access Article. Published on 05 August 2025. Downloaded on 5/7/2026 3:16:31 AM. This article is licensed under a Creative Commons Attribution 3.0 Unported Licence.

interactions between the hydrogen atoms in the triazine ring the halogen atoms in the XB donors as being present. The H···X interactions with the other donors in the 3 : 1 complexes, however, are roughly equal to what is observed from the 2 : 1 complexes.

Conclusions

The halogen and hydrogen bonding effects of $(C_3N_3R_3)\cdots(YBAX)_n$ complexes (R = H, OH, SH, or PH_2, Y = $(NO_2)_2$ or F_5, and n = 1, 2, or 3) were studied systematically at the M06-2X/aug-cc-pVDZ(-PP) (for I, Br) level of theory. The quantification of bond strength and qualitative representation of the halogen and supplemental hydrogen bonds were obtained through the application of local mode, NBO, and Bader's QTAIM analyses, respectively. As a result of these analyses, a few interesting results were observed:

(1) The X···N interaction was the largest contributor to the complex stability; however, complimentary hydrogen bonds add to the stability of the complex. Although weak in the majority of the complexes, the HBs approach intermediary strength based on the bond strength order obtained through local mode analyses.

(2) The addition of extra halogen bond donors to each complex shows that the interactions are less reliant upon polarization effects of the halogen atom and more reliant upon the supplementary hydrogen bonds and the hydrogen bond intermolecular separation.

(3) Each additional XB donor added to the XB complex results in approximately >90% additivity, or has a synergy <1 kcal mol^{-1}.

Ongoing studies taking advantage of different computational techniques for fundamental studies of noncovalent interactions are geared towards a better understanding for intermolecular interactions occurring in the XB acceptor molecules upon functional group substitution of the acceptor molecule. These studies will lead to new fundamental insights into the influence of crystal design and cooperative XB and HB interactions.

Author contributions

D. P. D. – data curation, formal analysis, investigation, visualization, writing – original draft; T. L. E. – conceptualization, methodology, software; K. L. S. – conceptualization, funding acquisition, project administration, resources, supervision, writing – review and editing.

Conflicts of interest

There are no conflicts to declare.

Data availability

Structural and electronic properties including key geometrical parameters (Tables S1–S11), supplemental counterpoise corrections (Tables S12–S15), and scatter plots of the binding energy and bond strength order *versus* local mode force constant (Fig. S1 and S2) for the XB complexes. See DOI: **https://doi.org/10.1039/d5cp02395e**

More data, such as output files, will be available upon request.

Acknowledgements

The authors were supported by the National Science Foundation (NSF) under award number 2147956. The authors thank Baylor University High Performance Research Computing services for their generous allocation of computational resources on the Kodiak HPC cluster and the CATCO Research group for the use of the Local Mode Analysis code.

References

1 R. S. Czarny, A. N. Ho and P. Shing Ho, *Chem. Rec.*, 2021, **21**, 1240–1251.
2 A. M. Montaña, *ChemistrySelect*, 2017, **2**, 9094–9112.
3 R. K. Rowe and P. S. Ho, *Acta Crystallogr., Sect. B: Struct. Sci., Cryst. Eng. Mater.*, 2017, **73**, 255–264.
4 G. Berger, P. Frangville and F. Meyer, *Chem. Commun.*, 2020, **56**, 4970–4981.
5 S. Benz, A. I. Poblador-Bahamonde, N. Low-Ders and S. Matile, *Angew. Chem., Int. Ed.*, 2018, **57**, 5408–5412.
6 G. Desiraju, *Acta Crystallogr., Sect. B: Struct. Sci., Cryst. Eng. Mater.*, 2019, **75**, 914–915.
7 G. Berger, J. Soubhye and F. Meyer, *Polym. Chem.*, 2015, **6**, 3559–3580.
8 J. S. Murray, G. Resnati and P. Politzer, *Faraday Discuss.*, 2017, **203**, 113–130.
9 M. Saccone and L. Catalano, *J. Phys. Chem. B*, 2019, **123**, 9281–9290.
10 M. K. Corpinot and D.-K. Bučar, *Cryst. Growth Des.*, 2019, **19**, 1426–1453.
11 K. T. Mahmudov, M. N. Kopylovich, M. F. C. Guedes da Silva and A. J. L. Pombeiro, *Coord. Chem. Rev.*, 2017, **345**, 54–72.
12 L. Vogel, P. Wonner and S. M. Huber, *Angew. Chem., Int. Ed.*, 2019, **58**, 1880–1891.
13 G. R. Desiraju and IUCr, *IUPAC definition of the hydrogen bond. Terminology and nomenclature*, 2017, **https://scripts.iucr.org/cgi-bin/paper?S2053273317092658**.
14 J. Quentin and L. R. MacGillivray, *ChemPhysChem*, 2020, **21**, 154–163.
15 P. Scilabra, G. Terraneo and G. Resnati, *Acc. Chem. Res.*, 2019, **52**, 1313–1324.
16 Y. Li, L. Meng, C. Sun and Y. Zeng, *J. Phys. Chem. A*, 2020, **124**, 3815–3824.
17 J. Bamberger, F. Ostler and O. G. Mancheño, *ChemCatChem*, 2019, **11**, 5198–5211.
18 J. Lu and S. Scheiner, *Molecules*, 2019, **24**, 2822.
19 M. S. Taylor, *Coord. Chem. Rev.*, 2020, **413**, 213270.

Open Access Article. Published on 05 August 2025. Downloaded on 5/7/2026 3:16:31 AM. This article is licensed under a Creative Commons Attribution 3.0 Unported Licence.

20 A. Frontera and A. Bauza, *Int. J. Mol. Sci.*, 2021, **22**, 12550.
21 R. Papagna, L. Vogel and S. M. Huber, *Anion-Binding Catalysis*, John Wiley & Sons, Ltd, 2022, pp. 307–343.
22 A. Docker, C. H. Guthrie, H. Kuhn and P. D. Beer, *Angew. Chem., Int. Ed.*, 2021, **60**, 21973–21978.
23 T. Clark, M. Hennemann, J. S. Murray and P. Politzer, *J. Mol. Model.*, 2007, **13**, 291–296.
24 P. Politzer, J. S. Murray, T. Clark and G. Resnati, *Phys. Chem. Chem. Phys.*, 2017, **19**, 32166–32178.
25 P. Politzer and J. S. Murray, *Crystals*, 2017, **7**, 212.
26 S. Scheiner, *J. Chem. Phys.*, 2020, **153**, 140901.
27 D. P. Devore, T. L. Ellington and K. L. Shuford, *J. Phys. Chem. A*, 2020, **124**, 10817–10825.
28 D. A. Decato, A. M. S. Riel, J. May, O. B. Berryman and IUCr, *Exploring the hydrogen bond enhanced halogen bond*, 2019, **https://scripts.iucr.org/cgi-bin/paper?S0108767319099161**.
29 D. A. Decato, A. M. S. Riel, J. H. May, V. S. Bryantsev and O. B. Berryman, *Angew. Chem., Int. Ed.*, 2021, **60**, 3685–3692.
30 S. Portela and I. Fernández, *Molecules*, 2021, **26**, 1885.
31 S. Scheiner, *J. Phys. Chem. A*, 2023, **127**, 4695–4703.
32 A. M. S. Riel, D. A. Decato, J. Sun and O. B. Berryman, *Chem. Commun.*, 2022, **58**, 1378–1381.
33 A. M. S. Riel, R. K. Rowe, E. N. Ho, A.-C. C. Carlsson, A. K. Rappé, O. B. Berryman and P. S. Ho, *Acc. Chem. Res.*, 2019, **52**, 2870–2880.
34 D. A. Decato, J. Sun, M. R. Boller and O. B. Berryman, *Chem. Sci.*, 2022, **13**, 11156–11162.
35 J. Sun, A. M. S. Riel and O. B. Berryman, *New J. Chem.*, 2018, **42**, 10489–10492.
36 A. M. S. Riel, D. A. Decato, J. Sun, C. J. Massena, M. J. Jessop and O. B. Berryman, *Chem. Sci.*, 2018, **9**, 5828–5836.
37 D. P. Devore, T. L. Ellington and K. L. Shuford, *J. Phys. Chem. A*, 2024, 1477–1490.
38 T. L. Ellington, D. P. Devore, W. M. Uvin, G. De Alwis, K. A. French and K. L. Shuford, *ChemPhysChem*, 2023, **24**, e202200812.
39 K. E. Riley, J. S. Murray, J. Fanfrlík, J. Řezáč, R. J. Solá, M. C. Concha, F. M. Ramos and P. Politzer, *J. Mol. Model.*, 2011, **17**, 3309–3318.
40 K. E. Riley, J. S. Murray, J. Fanfrlík, J. Řezáč, R. J. Solá, M. C. Concha, F. M. Ramos and P. Politzer, *J. Mol. Model.*, 2013, **19**, 4651–4659.
41 H. A. Bent, *Chem. Rev.*, 1961, **61**, 275–311.
42 S. T. Nguyen, T. L. Ellington, K. E. Allen, J. D. Gorden, A. L. Rheingold, G. S. Tschumper, N. I. Hammer and D. L. Watkins, *Cryst. Growth Des.*, 2018, **18**, 3244–3254.
43 D. Devore, T. Ellington and K. Shuford, *ChemPhysChem*, 2024, e202400607.
44 J. Lapp and S. Scheiner, *J. Phys. Chem. A*, 2021, **125**, 5069–5077.
45 F. F. Naghani, S. Emamian and K. Zare, *J. Phys. Org. Chem.*, 2021, **34**, e4213.
46 S. Scheiner and S. Hunter, *ChemPhysChem*, 2022, **23**, e202200011.
47 X. Wang, K. Maeda, A. Thomas, K. Takanabe, G. Xin, J. M. Carlsson, K. Domen and M. Antonietti, *Nat. Mater.*, 2009, **8**, 76–80.
48 V. W.-H. Lau and B. V. Lotsch, *Adv. Energy Mater.*, 2022, **12**, 2101078.
49 M. Ghashghaee, Z. Azizi and M. Ghambarian, *J. Phys. Chem. Solids*, 2020, **141**, 109422.
50 O. P. Olademehin, T. L. Ellington and K. L. Shuford, *J. Phys. Chem. A*, 2021, **125**, 7597–7606.
51 K. S. Lakhi, D.-H. Park, K. Al-Bahily, W. Cha, B. Viswanathan, J.-H. Choy and A. Vinu, *Chem. Soc. Rev.*, 2017, **46**, 72–101.
52 J. Liu, H. Wang and M. Antonietti, *Chem. Soc. Rev.*, 2016, **45**, 2308–2326.
53 L. Jiang, X. Yuan, Y. Pan, J. Liang, G. Zeng, Z. Wu and H. Wang, *Appl. Catal., B*, 2017, **217**, 388–406.
54 G. Dong, Y. Zhang, Q. Pan and J. Qiu, *J. Photochem. Photobiol., C*, 2014, **20**, 33–50.
55 W. Chen, T.-Y. Liu, T. Huang, X.-H. Liu and X.-J. Yang, *Nanoscale*, 2016, **8**, 3711–3719.
56 C. Xu, Q. Han, Y. Zhao, L. Wang, Y. Li and L. Qu, *J. Mater. Chem. A*, 2015, **3**, 1841–1846.
57 G. Dong, K. Zhao and L. Zhang, *Chem. Commun.*, 2012, **48**, 6178–6180.
58 Q. Han, C. Hu, F. Zhao, Z. Zhang, N. Chen and L. Qu, *J. Mater. Chem. A*, 2015, **3**, 4612–4619.
59 N. Sagara, S. Kamimura, T. Tsubota and T. Ohno, *Appl. Catal., B*, 2016, **192**, 193–198.
60 A. N. Petelski, D. J. R. Duarte, S. C. Pamies, N. M. Peruchena and G. L. Sosa, *Theor. Chem. Acc.*, 2016, **135**, 65.
61 K. Wang, D. Duan, M. Zhou, S. Li, T. Cui, B. Liu, J. Liu, B. Zou and G. Zou, *J. Phys. Chem. B*, 2011, **115**, 4639–4644.
62 S. Boys and F. Bernardi, *Mol. Phys.*, 1970, **19**, 553–566.
63 W. Tang, E. Sanville and G. Henkelman, *J. Phys.: Condens. Matter*, 2009, **21**, 084204.
64 E. Sanville, S. D. Kenny, R. Smith and G. Henkelman, *J. Comput. Chem.*, 2007, **28**, 899–908.
65 G. Henkelman, A. Arnaldsson and H. Jónsson, *Comput. Mater. Sci.*, 2006, **36**, 354–360.
66 M. Yu and D. R. Trinkle, *J. Chem. Phys.*, 2011, **134**, 064111.
67 J. P. Foster and F. Weinhold, *J. Am. Chem. Soc.*, 1980, **102**, 7211–7218.
68 A. E. Reed and F. Weinhold, *J. Chem. Phys.*, 1983, **78**, 4066–4073.
69 A. E. Reed and F. Weinhold, *J. Chem. Phys.*, 1985, **83**, 1736–1740.
70 A. E. Reed, R. B. Weinstock and F. Weinhold, *J. Chem. Phys.*, 1985, **83**, 735–746.
71 J. E. Carpenter and F. Weinhold, *THEOCHEM*, 1988, **169**, 41–62.
72 A. E. Reed, L. A. Curtiss and F. Weinhold, *Chem. Rev.*, 1988, **88**, 899–926.
73 F. Weinhold and J. E. Carpenter, *The Structure of Small Molecules and Ions*, Springer US, Boston, MA, 1988, pp. 227–236.
74 F. Weinhold and C. R. Landis, *Chem. Educ. Res. Pract.*, 2001, **2**, 91–104.

Open Access Article. Published on 05 August 2025. Downloaded on 5/7/2026 3:16:31 AM. This article is licensed under a Creative Commons Attribution 3.0 Unported Licence.

75 M. J. Frisch, G. W. Trucks, H. B. Schlegel, G. E. Scuseria, M. A. Robb, J. R. Cheeseman, G. Scalmani, V. Barone, G. A. Petersson, H. Nakatsuji, X. Li, M. Caricato, A. V. Marenich, J. Bloino, B. G. Janesko, R. Gomperts, B. Mennucci, H. P. Hratchian, J. V. Ortiz, A. F. Izmaylov, J. L. Sonnenberg, D. Williams-Young, F. Ding, F. Lipparini, F. Egidi, J. Goings, B. Peng, A. Petrone, T. Henderson, D. Ranasinghe, V. G. Zakrzewski, J. Gao, N. Rega, G. Zheng, W. Liang, M. Hada, M. Ehara, K. Toyota, R. Fukuda, J. Hasegawa, M. Ishida, T. Nakajima, Y. Honda, O. Kitao, H. Nakai, T. Vreven, K. Throssell, J. A. Montgomery, Jr., J. E. Peralta, F. Ogliaro, M. J. Bearpark, J. J. Heyd, E. N. Brothers, K. N. Kudin, V. N. Staroverov, T. A. Keith, R. Kobayashi, J. Normand, K. Raghavachari, A. P. Rendell, J. C. Burant, S. S. Iyengar, J. Tomasi, M. Cossi, J. M. Millam, M. Klene, C. Adamo, R. Cammi, J. W. Ochterski, R. L. Martin, K. Morokuma, O. Farkas, J. B. Foresman and D. J. Fox, *Gaussian~16 Revision C.01*, 2016.
76 Y. Zhao and D. G. Truhlar, *Theor. Chem. Acc.*, 2008, **120**, 215–241.
77 T. H. Dunning, Jr., *J. Chem. Phys.*, 1989, **90**, 1007–1023.
78 R. A. Kendall, T. H. Dunning and R. J. Harrison, *J. Chem. Phys.*, 1992, **96**, 6796–6806.
79 D. E. Woon and T. H. Dunning, *J. Chem. Phys.*, 1993, **98**, 1358–1371.
80 K. A. Peterson, D. Figgen, E. Goll, H. Stoll and M. Dolg, *J. Chem. Phys.*, 2003, **119**, 11113–11123.
81 K. A. Peterson, B. C. Shepler, D. Figgen and H. Stoll, *J. Phys. Chem. A*, 2006, **110**, 13877–13883.
82 S. Kozuch and J. M. L. Martin, *J. Chem. Theory Comput.*, 2013, **9**, 1918–1931.
83 A. Bauzá, I. Alkorta, A. Frontera and J. Elguero, *J. Chem. Theory Comput.*, 2013, **9**, 5201–5210.
84 T. Lu and F. Chen, *J. Comput. Chem.*, 2012, **33**, 580–592.
85 R. F. W. Bader, M. T. Carroll, J. R. Cheeseman and C. Chang, *J. Am. Chem. Soc.*, 1987, **109**, 7968–7979.
86 J. Stone, MSc thesis, Computer Science Department, University of Missouri-Rolla, 1998.
87 W. Humphrey, A. Dalke and K. Schulten, *J. Mol. Graphics*, 1996, **14**, 33–38.
88 R. M. Badger, *J. Chem. Phys.*, 1934, **2**, 128–131.
89 V. P. Oliveira, B. L. Marcial, F. B. C. Machado and E. Kraka, *Materials*, 2020, **13**, 55.
90 E. Kraka, W. Zou and Y. Tao, *Wiley Interdiscip. Rev.: Comput. Mol. Sci.*, 2020, **10**, e1480.
91 V. P. Oliveira, B. L. Marcial, F. B. C. Machado and E. Kraka, *Materials*, 2020, **13**, 55.
92 E. Kraka, J. A. Larsson and D. Cremer, *Computational Spectroscopy*, John Wiley & Sons, Ltd, 2010, ch. 4, pp. 105–149.
93 R. Kalescky, E. Kraka and D. Cremer, *J. Phys. Chem. A*, 2013, **117**, 8981–8995.
94 E. Kraka, D. Setiawan and D. Cremer, *J. Comput. Chem.*, 2016, **37**, 130–142.
95 D. Setiawan, D. Sethio, D. Cremer and E. Kraka, *Phys. Chem. Chem. Phys.*, 2018, **20**, 23913–23927.
96 V. Oliveira, E. Kraka and D. Cremer, *Phys. Chem. Chem. Phys.*, 2016, **18**, 33031–33046.
97 S. Yannacone, V. Oliveira, N. Verma and E. Kraka, *Inorganics*, 2019, **7**, 47.
98 V. Oliveira, D. Cremer and E. Kraka, *J. Phys. Chem. A*, 2017, **121**, 6845–6862.
99 D. Setiawan, E. Kraka and D. Cremer, *J. Phys. Chem. A*, 2015, **119**, 9541–9556.
100 M. Freindorf, E. Kraka and D. Cremer, *Int. J. Quantum Chem.*, 2012, **112**, 3174–3187.
101 R. Kalescky, W. Zou, E. Kraka and D. Cremer, *Chem. Phys. Lett.*, 2012, **554**, 243–247.
102 R. Kalescky, E. Kraka and D. Cremer, *Mol. Phys.*, 2013, **111**, 1497–1510.
103 Y. Tao, W. Zou, J. Jia, W. Li and D. Cremer, *J. Chem. Theory Comput.*, 2017, **13**, 55–76.
104 Y. Tao, W. Zou and E. Kraka, *Chem. Phys. Lett.*, 2017, **685**, 251–258.
105 W. Zou, Y. Tao, M. Freindorf, M. Makos, N. Verma and E. Kraka, *LMODEA2020*, 2022.
106 Z. Konkoli and D. Cremer, *Int. J. Quantum Chem.*, 1998, **67**, 1–9.
107 E. Kraka and D. Cremer, *Int. J. Quantum Chem.*, 2019, **119**, e25849.
108 Y. Tao, W. Zou, S. Nanayakkara and E. Kraka, *J. Chem. Theory Comput.*, 2022, **18**, 1821–1837.
109 B. Bankiewicz and M. Palusiak, *Symmetry*, 2021, **13**, 766.
110 L. de Azevedo Santos, D. Cesario, P. Vermeeren, S. C. C. van der Lubbe, F. Nunzi and C. Fonseca Guerra, *ChemPlusChem*, 2022, **87**, e202100436.
111 X. C. Yan, P. Schyman and W. L. Jorgensen, *J. Phys. Chem. A*, 2014, **118**, 2820–2826.
112 R. D. Parra, *Chem. Phys. Lett.*, 2022, **803**, 139825.
113 N. Bedeković, T. Piteša, M. Eraković, V. Stilinović and D. Cinčić, *Cryst. Growth Des.*, 2022, **22**, 2644–2653.
114 M. Côté, J. S. Ovens and D. L. Bryce, *Chem. – Asian J.*, 2023, **18**, e202201221.